LIGHT METALS

Large plasticity in magnesium mediated by pyramidal dislocations

Bo-Yu Liu[1]*, Fei Liu[1]*, Nan Yang[1], Xiao-Bo Zhai[2], Lei Zhang[3], Yang Yang[4], Bin Li[4]†, Ju Li[5], Evan Ma[6], Jian-Feng Nie[7,8]†, Zhi-Wei Shan[1]†

Lightweight magnesium alloys are attractive as structural materials for improving energy efficiency in applications such as weight reduction of transportation vehicles. One major obstacle for widespread applications is the limited ductility of magnesium, which has been attributed to $\langle c+a \rangle$ dislocations failing to accommodate plastic strain. We demonstrate, using in situ transmission electron microscope mechanical testing, that $\langle c+a \rangle$ dislocations of various characters can accommodate considerable plasticity through gliding on pyramidal planes. We found that submicrometer-size magnesium samples exhibit high plasticity that is far greater than for their bulk counterparts. Small crystal size usually brings high stress, which in turn activates more $\langle c+a \rangle$ dislocations in magnesium to accommodate plasticity, leading to both high strength and good plasticity.

Magnesium is the lightest structural metal, with a density about 35% and 77% less than that of aluminum and steel, respectively (*1*). Magnesium alloys are actively being developed because of their potential usefulness for improving energy efficiency across the automobile, aircraft, and aerospace industries, in which the weight savings translate to lower energy consumption. However, the generally limited ductility of Mg at room temperature makes the processing and forming of profiles and components difficult and costly. Consequentially, low ductility has become one major obstacle that hampers the widespread applications of Mg products.

The ductility of Mg is intimately related to the fundamental behaviors of pyramidal $\langle c+a \rangle$ dislocations (fig. S1), which are the major contributor to *c*-axis strain (*2*, *3*). High ductility of Mg should therefore be achievable by generating more $\langle c+a \rangle$ dislocations (*4*–*7*). However, $\langle c+a \rangle$ dislocations are thought to be intrinsically unstable by readily transforming into sessile structures that cannot contribute to plastic strain (*8*–*10*). In light of this generally accepted understanding, proposed alloy design strategies primarily stabilize the $\langle c+a \rangle$ dislocation and prevent the glissile-to-sessile transformation (*11*). The glissile-to-sessile transformation is not observed in some recent simulation studies (*12*–*14*), in which $\langle c+a \rangle$ dislocations glide on pyramidal planes, even though the actual slip plane is under debate (*15*, *16*). Controversy surrounds the fundamental behavior of $\langle c+a \rangle$ dislocations, such as their ability to accommodate plastic strain and their slip pathways. This creates difficulties in rationalizing the mechanical behavior and for alloy design. We exploited in situ transmission electron microscope (TEM) mechanical testing (*17*, *18*), three-dimensional (3D) image reconstruction, and atomistic simulations to resolve the prevailing uncertainties. Our results document large plastic strains mediated by abundant $\langle c+a \rangle$ dislocations gliding on both pyramidal I $\{10\bar{1}1\}$ and pyramidal II $\{11\bar{2}2\}$ planes.

We performed in situ TEM mechanical testing at room temperature on submicrometer-size pillars of Mg single crystals (table S1). The pillars were fabricated by focused ion beam milling and tested inside TEM (fig. S2). We compressed the pillars along their *c* axis (Fig. 1 and movie S1), with the misalignment angle at less than 5°. In this condition, the $\langle c \rangle$ or $\langle a \rangle$ dislocation slip and $\{10\bar{1}2\}$ deformation twinning are all difficult to generate. We also conducted controlled experiments with the electron beam switched off and confirmed that the electron beam we used had no obvious effect on the mechanical behavior of the tested samples (fig. S3). We performed $\mathbf{g} \cdot \mathbf{b}$ analyses (where $\mathbf{g}$ is the diffraction vector and $\mathbf{b}$ is the Burgers vector) to determine the Burgers vector of dislocations (*19*).

All the pillars we tested underwent uniform deformation and exhibited fairly large dislocation-mediated plastic strains without failure (Fig. 1 and fig. S4). Dislocations were generated successively from the top region of the pillar, propagated gradually toward the bottom part of the pillar. With further deformation of the pillar, individual dislocations became difficult to image because their density was too high (Fig. 1C); therefore, we found it hard to analyze the Burgers vectors of these dislocations. To circumvent this difficulty, we used trapezoidal-shaped samples to generate

[1]Center for Advancing Materials Performance from the Nanoscale (CAMP-Nano) and Hysitron Applied Research Center in China (HARCC), State Key Laboratory for Mechanical Behavior of Materials, Xi'an Jiaotong University, Xi'an 710049, People's Republic of China. [2]College of Science, Xi'an University of Science and Technology, Xi'an 710054, People's Republic of China. [3]MOE Key Laboratory for Nonequilibrium Synthesis and Modulation of Condensed Matter, School of Science, Xi'an Jiaotong University, Xi'an 710049, People's Republic of China. [4]Department of Chemical and Materials Engineering, University of Nevada, Reno, NV 89557, USA. [5]Departments of Nuclear Science and Engineering and Materials Science and Engineering, Massachusetts Institute of Technology, Cambridge, MA 02139, USA. [6]Department of Materials Science and Engineering, Johns Hopkins University, Baltimore, MD 21218, USA. [7]Department of Materials Science and Engineering, Monash University, Melbourne, Victoria, 3800, Australia. [8]International Joint Laboratory for Light Alloys (Ministry of Education), College of Materials Science and Engineering, Chongqing University, Chongqing 400044, People's Republic of China.
*These authors contributed equally to this work.
†Corresponding author. Email: zwshan@xjtu.edu.cn (Z.-W.S.); jianfeng.nie@monash.edu (J.-F.N.); binl@unr.edu (B.L.)

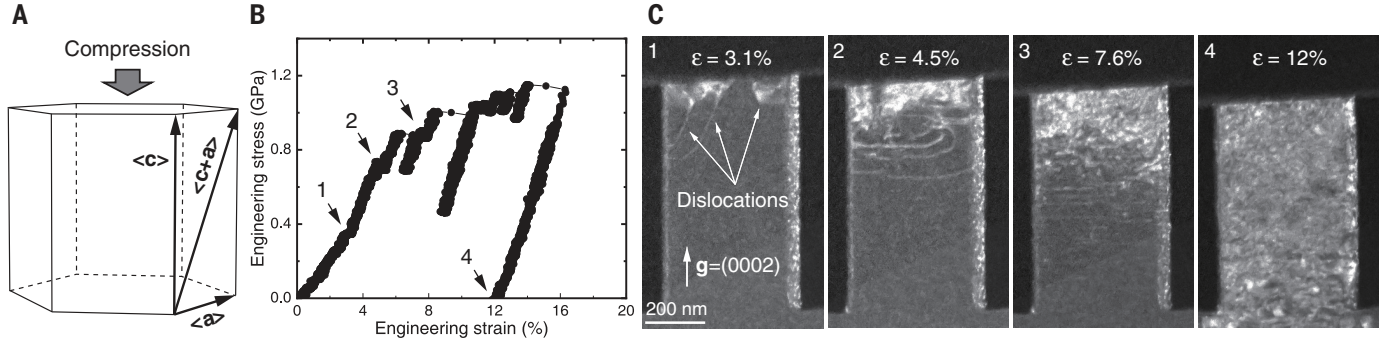

Fig. 1. In situ TEM compression test showing that dislocation slip is responsible for the plastic deformation of an Mg single-crystal pillar under *c*-axis compression. (**A**) Hexagonal unit cell showing the loading orientation. (**B**) Stress-strain curve. (**C**) Snapshots showing an increase in dislocation density during compression. The dark-field TEM observation is conducted under a two-beam condition. Electron beam direction ~$[\bar{2}110]$ (*a* axis). ε, engineering strain.

a stress gradient from the sample top to root (Fig. 2). During compression, we retracted the flat punch once dislocations appeared at the root (movie S2). Although the top was severely deformed, and its image contrast was complex, dislocations in regions near the sample root were all clearly visible. The Burgers vectors of these dislocations have both $\langle c \rangle$ and $\langle a \rangle$ components, and hence they are $\langle c + a \rangle$. Presumably, the generation and slip of the $\langle c + a \rangle$ dislocations effectively accommodates the plastic strain.

The $\langle c + a \rangle$ dislocations we observed in our study usually exhibited half-loop and zig-zag configurations (fig. S5A), similar to the $\langle c + a \rangle$ dislocations observed in bulk Mg (*4*, *20*–*22*). We believe the existence of such configurations suggests that $\langle c + a \rangle$ dislocations have both edge and screw characters and are thus of mixed type. The half loop shown in Fig. 3A formed at the top-right corner of the pillar and expanded continuously toward the lower-left corner during straining until it reached the pillar surface (fig. S6 and movie S3). This observation indicated to us that the $\langle c + a \rangle$ mixed dislocations are glissile, contributing to the plastic deformation, implying that $\langle c + a \rangle$ edge and screw dislocations are also glissile. For some $\langle c + a \rangle$ dislocations, some of their segments lie parallel to the intersection of pyramidal and basal planes and are also perpendicular to the Burgers vector. Hence, they are of edge type (see geometry analyses in fig. S5). Such edge segments are glissile (Fig. 3B and movie S4). Examination of other half loops and edge segments indicated that they are all glissile (fig. S7 and movie S5). Moreover, we observed reversible motion of $\langle c + a \rangle$ dislocations under cyclic loading (fig. S8 and movie S6). This indicates that the $\langle c + a \rangle$ dislocations retained their identity and mobility rather than becoming sessile. The mobility of the $\langle c + a \rangle$ dislocations was further supported by our atomistic simulation in which $\langle c + a \rangle$ dislocations nucleated during *c*-axis compression and glided on the pyramidal planes (figs. S9 and S10 and movie S7).

The straight segments lying parallel to the pyramidal-basal intersection were reported previously (*20*). The presence of such long segments has been attributed to low mobility of $\langle c + a \rangle$ edge dislocations (*20*), formation of sessile dislocation locks along the pyramidal-basal intersection (*23*), and dissociation of $\langle c + a \rangle$ dislocations into partials and basal stacking fault (*8*). Here, we propose that such rectilinear configuration can also result from the formation of dislocation dipole (Fig. 3C and movie S5). A straight dislocation dipole can form when a dislocation is pinned (marked by the yellow cross). The arrangement of the dipole and its two neighboring segments, 1 and 2, gave rise to an ε shape. Under the applied stress, segments 1 and 2 glided toward the left, accompanied by the elongation of the dipole. The geometry analysis indicated that this dipole was pure edge. During further straining, segments 1 and 2 formed a junction, leaving debris behind. The dislocation dipole and debris were both sessile, which can serve as obstacles to other dislocations. A likely mechanism for dipole formation by way of cross-slip is shown in fig. S11, similar to what has been proposed in other hexagonal structures such as zinc (*24*).

The formation of such a dislocation dipole requires cross-slip between two different pyramidal planes. Comparison of these two pyramidal planes is shown in fig. S12. Although the cross-slip of $\langle c + a \rangle$ dislocations between pyramidal I and II planes was studied in a computer simulation (*25*), cross-slip has not been unambiguously confirmed by experiments. Traditionally, the $\langle c + a \rangle$ slip plane is determined by slip-trace analyses, which is usually compounded by the lack of 3D information. We used a series of TEM images to construct 3D tomography to reveal the configuration and slip plane of $\langle c + a \rangle$ dislocation (fig. S13 and movies S8 and S9). Figure 4 shows 3D tomography of three $\langle c + a \rangle$ dislocations generated in *c*-axis compression. All three dislocations exhibit a curvilinear shape, indicating that they are mixed dislocations. When the pyramidal II plane is edge on, the projection of dislocation 1 becomes straight and lies on the trace of the pyramidal II plane, indicating that its gliding plane is pyramidal II (Fig. 4B). Similarly, the slip plane of dislocation 3 is pyramidal I (Fig. 4C). Dislocation 2 lies on two adjacent pyramidal II planes, indicating that cross-slip occurred. Further gliding of its segments on the two pyramidal planes would generate a dislocation dipole.

Our submicrometer-size Mg single crystals exhibit both higher strength and plasticity than

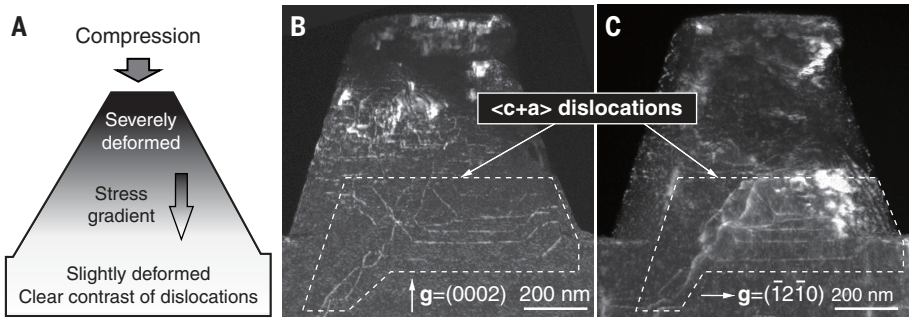

Fig. 2. Diffraction contrast analyses of $\langle c + a \rangle$ dislocations in a deformed trapezoidal sample. (**A**) Schematic illustration of the testing configuration. The pillar root is four times larger than the top. (**B** and **C**) Dark-field TEM images recorded from the same region. Electron beam direction ~[1̄010].

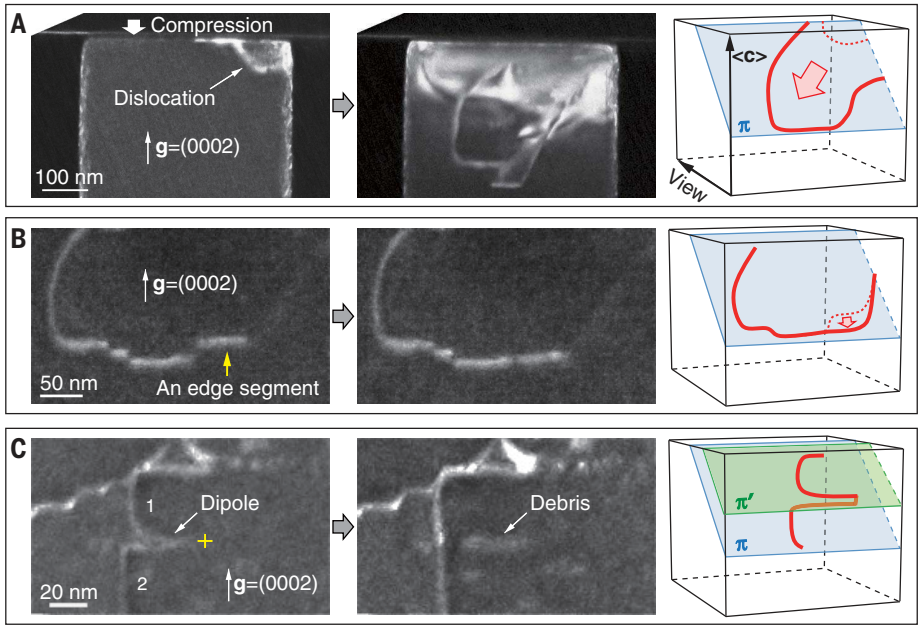

Fig. 3. In situ TEM showing the motion of $\langle c + a \rangle$ dislocations in different samples. (**A**) Expansion of a half loop. (**B**) Motion of an edge segment. (**C**) Formation of a dislocation dipole and debris. Electron beam direction ~[2̄110]. Schematic drawings of the moving dislocations are shown right to the TEM images. Symbol π refers to the pyramidal plane, and π′ is an adjacent pyramidal plane parallel to π. The red dashed line refers to the previous location of the moving dislocation.

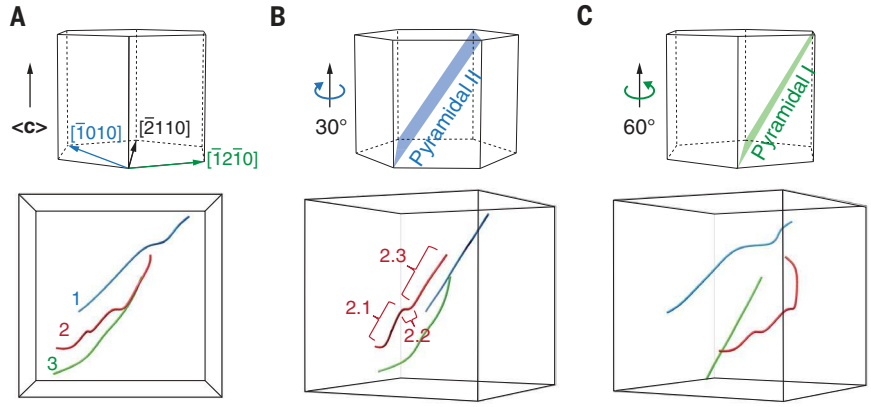

Fig. 4. 3D reconstruction revealing the pyramidal I and II gliding planes and cross-slip of $\langle c + a \rangle$ dislocations. The hexagonal unit cells indicate the viewing directions and the two pyramidal planes. (**A**) Viewing direction is [$\bar{2}$110]. Three curvilinear dislocations are selected for 3D analyses. (**B**) Viewing direction is [$\bar{1}$010]. In this orientation, the pyramidal II plane is edge on. Dislocation 1 is projected as a straight line, and hence, its slip plane is pyramidal II. For dislocation 2, segments 2.1 and 2.3 lie in different but nearby pyramidal II planes, indicating cross-slip of this dislocation. (**C**) Viewing direction is [$\bar{1}2\bar{1}0$]. The pyramidal I plane is edge on. Dislocation 3 is projected as a straight line, and therefore, its slip plane is pyramidal I.

their bulk counterpart (*26*), leading to a phenomenon of "smaller is stronger and more ductile." This phenomenon likely originates from the following factors. Small crystals usually have few preexisting dislocations, and therefore, a large amount of stress is required to nucleate dislocations. Once nucleated, dislocations can readily escape to the surfaces before dislocation multiplication, necessitating increasing stress levels to nucleate other dislocations or activate other dislocation sources to continue plasticity. Such size effects result in high stress in submicrometer-size Mg, which in turn activates abundant $\langle c + a \rangle$ dislocations to accommodate more plasticity. Another reason for the good plasticity is the rich surface sources for dislocations per unit volume, due to the large surface-to-volume ratio, which enables profuse dislocations to be generated successively from the crystal surface. Moreover, deformation twinning, which often occurs in bulk Mg under *c*-axis straining and introduces shear localization and stress concentration (*27*), is not seen in our pillars. Therefore, no potential twin-induced crack initiation sites exist in the pillars, which may also contribute to the improved plasticity. Furthermore, in a more general case, the stress concentration associated with a flaw in the tiny crystal is expected to be small, as the stress concentration factor is related to the flaw length over the flaw-tip radius. Our small crystal dimension limits this flaw aspect ratio. This prevents premature failure and allows the small crystal to maximize its potential ductility.

Our findings provide information on the mobility of pyramidal dislocations and its relationship with plasticity in pure Mg of small sizes, as well as insights into strategies for achieving long-sought plasticity in Mg that is traditionally difficult to form at room temperature. Simultaneously promoting dislocations and suppressing deformation twinning can be an effective strategy in this regard. Our experimental strategy can be extended to understanding the behavior of other hexagonal metals by identifying which microstructures promote or degrade properties such as strength and ductility.

REFERENCES AND NOTES

1. T. M. Pollock, *Science* **328**, 986–987 (2010).
2. M. H. Yoo, *Metall. Mater. Trans. A* **12**, 409–418 (1981).
3. S. Agnew, D. Brown, C. Tome, *Acta Mater.* **54**, 4841–4852 (2006).
4. S. Sandlöbes *et al.*, *Acta Mater.* **60**, 3011–3021 (2012).
5. S. Sandlöbes *et al.*, *Acta Mater.* **70**, 92–104 (2014).
6. S. R. Agnew, L. Capolungo, C. A. Calhoun, *Acta Mater.* **82**, 255–265 (2015).
7. S. Sandlöbes *et al.*, *Sci. Rep.* **7**, 10458 (2017).
8. Z. Wu, W. A. Curtin, *Nature* **526**, 62–67 (2015).
9. Z. Wu, W. A. Curtin, *Scr. Mater.* **116**, 104–107 (2016).
10. R. Ahmad, Z. Wu, S. Groh, W. A. Curtin, *Scr. Mater.* **155**, 114–118 (2018).
11. Z. Wu, R. Ahmad, B. Yin, S. Sandlöbes, W. A. Curtin, *Science* **359**, 447–452 (2018).
12. Y. Tang, J. A. El-Awady, *Acta Mater.* **71**, 319–332 (2014).
13. A. Kumar, B. M. Morrow, R. J. McCabe, I. J. Beyerlein, *Mater. Sci. Eng. A* **695**, 270–278 (2017).
14. Z. Ding *et al.*, *Acta Mater.* **146**, 265–272 (2018).
15. H. Fan, J. A. El-Awady, *Mater. Sci. Eng. A* **644**, 318–324 (2015).
16. K. Y. Xie, Z. Alam, A. Caffee, K. J. Hemker, *Scr. Mater.* **112**, 75–78 (2016).
17. B. Y. Liu *et al.*, *Nat. Commun.* **5**, 3297 (2014).
18. B.-Y. Liu *et al.*, *J. Mater. Sci. Technol.* **34**, 1061–1066 (2018).
19. Materials and methods are available as supplementary materials.
20. T. Obara, H. Yoshinga, S. Morozumi, *Acta Metall.* **21**, 845–853 (1973).
21. J. Geng, M. F. Chisholm, R. K. Mishra, K. S. Kumar, *Philos. Mag.* **95**, 3910–3932 (2015).
22. J. Jain, P. Cizek, K. Hariharan, *Scr. Mater.* **130**, 133–137 (2017).
23. B. Li, Q. W. Zhang, S. N. Mathaudhu, *Scr. Mater.* **134**, 37–41 (2017).
24. P. B. Price, *Philos. Mag.* **5**, 873–886 (1960).
25. M. Itakura, H. Kaburaki, M. Yamaguchi, T. Tsuru, *Phys. Rev. Lett.* **116**, 225501 (2016).
26. C. M. Byer, B. Li, B. Cao, K. T. Ramesh, *Scr. Mater.* **62**, 536–539 (2010).
27. M. R. Barnett, *Mater. Sci. Eng. A* **464**, 8–16 (2007).

ACKNOWLEDGMENTS

We acknowledge Z. Zhang (Hefei University of Technology) for providing the Mg single crystals; Q. J. Li (Johns Hopkins University) for fruitful discussions; and P. Zhang, C. W. Guo, and D. L. Zhang (Xi'an Jiaotong University) for assistance in focused ion beam and TEM experiments. We also appreciate the support from the International Joint Laboratory for Micro/Nano Manufacturing and Measurement Technologies and the Collaborative Innovation Center of High-End Manufacturing Equipment. **Funding:** The authors acknowledge the support from the National Key Research and Development Program of China (2017YFB0702001), National Natural Science Foundation of China (51601141, 51621063, 11504290, and 11834018), 111 Project 2.0 (BP2018008), China Postdoctoral Science Foundation (2016M600788), and the Science and Technology Department of Shaanxi Province (2016KTZDGY-04-03 and 2016KTZDGY-04-04). E.M. was supported by the U.S. Department of Energy (BES-DMSE no. DE-FG02-16ER46056). B.L. acknowledges the support from U.S. National Science Foundation (CMMI-1635088). J.-F.N. acknowledges the support from the Australian Research Council. J.L. was supported by NSF DMR-1410636. **Author contributions:** J.-F.N. and Z.-W.S. designed and supervised the project. B.-Y.L., F.L., and N.Y. performed the in situ TEM experiments and carried out the data analysis. X.-B.Z., B.-Y.L., and L.Z. carried out the 3D image reconstruction. Y.Y. and B.L. carried out the simulation and interpreted the results. J.L. and E.M. contributed to the interpretations of the observations. B.-Y.L., J.-F.N., B.L., E.M., and Z.-W.S. wrote the paper. All authors contributed to discussions of the results. **Competing interests:** The authors declare no competing interests. **Data and materials availability:** All data are available in the manuscript or the supplementary materials.

SUPPLEMENTARY MATERIALS

science.sciencemag.org/content/365/6448/73/suppl/DC1
Materials and Methods
Figs. S1 to S13
Table S1
Movies S1 to S9
References (*28*–*32*)

5 December 2018; accepted 8 May 2019
10.1126/science.aaw2843

Science

Large plasticity in magnesium mediated by pyramidal dislocations

Bo-Yu Liu, Fei Liu, Nan Yang, Xiao-Bo Zhai, Lei Zhang, Yang Yang, Bin Li, Ju Li, Evan Ma, Jian-Feng Nie and Zhi-Wei Shan

Science **365** (6448), 73-75.
DOI: 10.1126/science.aaw2843

Smaller but more ductile

Poor ductility is one limiting factor in widespread use of strong but lightweight magnesium alloys in cars, trains, and planes. The usual way to try to circumvent this poor ductility is by adding other elements, which can be costly. Liu *et al.* show that very small samples of pure magnesium are much more ductile than previously believed (see the Perspective by Proust). The small samples suppress the deformation twinning that causes fractures in larger samples. Avoiding this mechanism should allow development of high-ductility magnesium and other metal alloys.

Science, this issue p. 73; see also p. 30